ACCEPTED MANUSCRIPT
Physics of Fluids
AIP Publishing
This is the author's peer reviewed, accepted manuscript. However, the online version of record will be different from this version once it has been copyedited and typeset.
PLEASE CITE THIS ARTICLE AS DOI: 10.1063/5.0249587

An Electromagnetic Logic Metastructure Realizing Half Addition and Half Subtraction Operations Based on Virtual Polarizer

Jia-Hao Zou (邹家豪), Jun-Yang Sui (眭钧阳), and Hai-Feng Zhang (章海锋)[a)]

College of Electronic and Optical Engineering & College of Flexible Electronics (Future Technology), Nanjing University of Posts and Telecommunications, Nanjing, 210023, China

Abstract-An electromagnetic logic metastructure (ELM) based on the virtual polarizer, capable of realizing half addition and half subtraction operations, is presented in this work. A virtual polarizer can control the polarization state of electromagnetic waves by coherent perfect absorption. Electromagnetic waves display their distinctive propagation characteristics in diverse polarization directions through the utilization of anisotropic materials such as liquid crystal and plasma, enabling the ELM to fulfill the function of the virtual polarizer. Through changing the physical quantities regarded as inputs, a transmission peak or an absorption peak is formed in different polarization directions when the logical relation is met. The parallel solution of the AND logic and XOR logic operations is realized, and achieve the function of half addition and half subtraction. The AxialRatio proves that the calculation results can be quickly solved by observing the different polarization states of the waves. The ELM based on the virtual polarizer processes data faster and more accurately than traditional logic devices. Half addition and half subtraction operations realized based on different electromagnetic polarization offer a novel approach to control the propagation of electromagnetic waves. It might have significant implications for the application of liquid crystal and other anisotropic materials.

I. INTRODUCTION

Electromagnetic signal processing techniques may be required for future high-performance and ultrahigh-speed logical networks[1,2]. Realizing logical operation based on electromagnetic signals is one of the important research directions[3,4]. The aim of the half-addition operation is to export a sum bit (S) and a carry bit (C)[5]. The half subtraction operation is used to output a difference bit (D) and a borrow bit (B)[6]. Their truth tables are shown in TABLE I (The binary numbers of the two inputs are defined as X and Y). Due to their applications in binary counters[7] and the encryption and decryption of secure network data[5,8], the study of achieving more efficient and reliable electromagnetic half-adders and half-subtractors has attracted widespread attention[9,10].

Metastructures are artificially engineered, periodic structures[11,12]. The exploration of exotic wave phenomena within metastructures and their wide-ranging applications represent one of the most intensively studied areas in the field of electromagnetic waves (EWs), covering frequencies from radio to optics[13-17]. Controlling EWs interactions—incorporating areas such as nonlinear optics[18], semiconductor physics[19], two-dimensional materials[20], and soft matter[21]—is one of the most intriguing possibilities for wave engineering with metastructures. Additionally,

a) Corresponding author at: College of Electronic and Optical Engineering & College of Flexible Electronics (Future Technology), Nanjing University of Posts and Telecommunications, Nanjing, 210023 ,China
E-mail: hanlor@163.com or hanlor@njupt.edu.cn

ACCEPTED MANUSCRIPT
Physics of Fluids
AIP Publishing
This is the author's peer reviewed, accepted manuscript. However, the online version of record will be different from this version once it has been copyedited and typeset.
PLEASE CITE THIS ARTICLE AS DOI: 10.1063/5.0249587

electromagnetic logic metastructures (ELM) offer advantages in electromagnetic image processing[22] and complex logic operations[23], drawing increasing attention as a novel approach to achieving electromagnetic logic[24].

TABLE I The truth table of half addition and half subtraction

INPUTS		**OUTPUTS**			
		Half Addition		Half Subtraction	
X	***Y***	**Sum (*X* add *Y*)**	**Carry (*X* add *Y*)**	**Difference (*X* minus *Y*)**	**Borrow (*X* minus *Y*)**
0	0	0	0	0	0
0	1	1	0	1	1
1	0	1	0	1	0
1	1	0	1	0	0

Coherent perfect absorption (CPA), with significant potential for use in electromagnetic devices, has been an attractive area of study[25]. The CPA is based on the principles of electromagnetic interference[26]. By precisely controlling the phase difference and intensities between the coherent EWs, CPA, compared to single-port incidence, can improve the ratio of absorptivity. Because this technology is based on the principles of electromagnetic interference, which is a common physical phenomenon, it may be used in a wide range of structures and materials[27]. Therefore, CPA provides a new direction for research on the electromagnetic application of soft materials such as liquid crystals[28].

So, it has been the subject of in-depth research in recent years. Dey *et al*.[27] proposed a scheme for high-precision position sensing based on CPA in a composite multi-layered structure. Achieve the high-precision position sensing based on periodic CPA resonances. Hasegawa *et al.*[28] successfully observed the CPA phenomenon in liquid thin films for the first time and demonstrated that CPA is a sensitive measurement method for detecting the optical anisotropy of thin films. Markowitz *et al*.[29] proposed a multilayer absorber with CPA. Because it can effectively capture monochromatic EWs from a wide incidence angle, the device can realize efficient electromagnetic power transmission. It is undeniable that these works prove the advantages of CPA in realizing optical devices, especially sensing. However, there is a lack of research on the ELM based on CPA[24,30].

Although there are some works about ELM realizing logic gates, the research of arithmetic logic units like half-adders and half-subtractors based on ELM is also blank[24,30]. Moreover, based on the technology of CPA, Wu *et al*. have proposed a novel concept, a virtual polarizer[31], which can manipulate the polarization of EWs. It will be interesting to combine a virtual polarizer with arithmetic operations in an ELM. This can not only realize the control of polarization and phase[31] but also improve the efficiency of ELM[32]. The application prospect of ELM in the field of antennas and propagation is greatly improved[31,32].

Herein, a layered one-dimensional electromagnetic logic metastructure (ELM) that performs half-addition and half-subtraction operations is presented. Utilizing anisotropic materials like liquid crystals (detailed in Section 1 of the supplementary material) and plasma, electromagnetic waves (EWs) exhibit unique propagation characteristics in both transverse electric (TE) and transverse magnetic (TM) modes (definitions provided in Ref.32 and Ref.33), like a virtual polarizer. In TE mode, the input logic level is modulated by adjusting the applied electric fields. A sharp transmission peak (TP) appears when the output level equals "1." For TM mode, the phase and applied magnetic fields serve as input parameters. When the phase and amplitude conditions for CPA are met, a sharp absorption peak (AP) is generated by the ELM[26,32]. The transition between half-addition and half-subtraction is achieved by adjusting the phase difference of coherent EWs. The two output bits for these operations are calculated independently in different polarization modes, allowing the ELM to perform both logical operations simultaneously, thus functioning as an electromagnetic half-adder or half-subtractor. Moreover, the resulting peaks have

ACCEPTED MANUSCRIPT
Physics of Fluids
AIP Publishing
This is the author's peer reviewed, accepted manuscript. However, the online version of record will be different from this version once it has been copyedited and typeset.
PLEASE CITE THIS ARTICLE AS DOI: 10.1063/5.0249587

high-quality factors (Q), reaching up to 3.6×10^3 and 1.2×10^4, respectively. The ELM demonstrates a strong signal-to-noise ratio (SNR)[34] for both logical operations, achieving at least 28 dB. So, the electromagnetic logic operations based on different polarizations are steady and quick. Owing to the constraints of experimental conditions and funds, mathematical computations[35,36] and the numerical verification based on "High-Frequency Simulator Structure (HFSS)" simulation software constitute the primary content of this paper rather than experimental verification.

II. STRUCTURE DESIGN AND THEORETICAL CALCULATION

A. The configuration of ELM

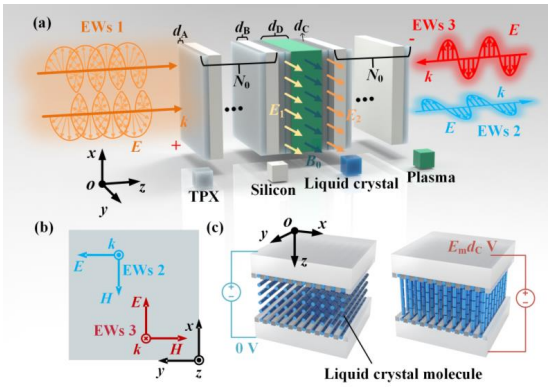

Fig. 1. Schematic diagram of the proposed ELM. (a) The ELM is made up of different dielectric layers, circularly polarized EWs 1 incidents from the positive side (+), linear polarization EWs 2 transmits from the negative side (-), and linear polarization EWs 3 incidents from the negative side. (b) EWs 2 transmits in TE mode and EWs 3 incidents in TM mode. (c) By applying different voltages, the long molecular axis of the liquid crystal is parallel to different directions (the positive direction of the y-axis or the positive direction of the z-axis).

TABLE II The detailed parameters of the ELM

Parameters	d_A	d_B	d_C	d_D	N_0
Value	2 mm	4 mm	0.2 mm	10 mm	12

The ELM in this paper is a one-dimensional layered structure, as can be seen in Fig. 1(a), and different materials are represented by different colors. Although this work focuses on theoretical research, this ELM can be manufactured with the help of physical vapor deposition[37] or wet etching[38] (Supplement material section 2 provides a detailed introduction to the particular procedure). The ELM is made up of Methyl pentene copolymer (TPX)[39], Silicon (Si)[40], plasma[33], and liquid crystal. The thicknesses of the different dielectric layers are defined as d_A, d_B, d_C, and d_D, respectively. The detailed parameters of the proposed ELM are listed in TABLE II. TPX is a polymer material, and its refractive index (RI) is regarded as 1.44 in this paper[39]. Si is widely studied in the field of electromagnetic because of its high RI (n_B=3.4)[40]. The two isotropic dielectrics are periodically layered, and the number of layered periods is regarded as N_0. After parameter optimization, mentioned below, the ELM has the best performance when N_0 is set as 12.

Fig. 1(a) displays that circularly polarized EWs 1 illuminates the positive side of the ELM (since the results are

ACCEPTED MANUSCRIPT
Physics of Fluids
AIP Publishing
This is the author's peer reviewed, accepted manuscript. However, the online version of record will be different from this version once it has been copyedited and typeset.
PLEASE CITE THIS ARTICLE AS DOI: 10.1063/5.0249587

the same, left or right circular polarization is not considered in this paper). When the wave vector k propagates along the positive z-axis, the TE mode refers to the positive y-axis being considered as the positive direction of the electric field E of EWs and the negative x-axis being regarded as the positive direction of magnetic field H. The TM mode is defined as the polarization mode where the E is in the x-o-z plane and the H is along the negative y-axis when EWs propagate along the negative z-axis. As seen in Fig. 1(b), EWs 2 transmits in TE mode, and the positive direction of E is along the positive direction of the y-axis. The EWs 2 is in TM mode, and the positive direction of E is along the positive direction of the x-axis due to vertical incidence.

B. The RIs of plasma in TE and TM modes

The dielectric of plasma exhibits an anisotropic material due to the external magnetic field, and so, its RI in TM mode varies with the magnetic field strength[41]. Xuan *et al.*[42] proposed a work about producing a spatial linear magnetic field by applying current to a coil. It provides a way to apply the external magnetic field (B_0).

As shown in Fig. 1(a), the applied B_0 is parallel to the positive y-axis (the other layers in this paper are unaffected by B_0). The dielectric tensor of plasma can be given by the matrix as[33]:

$$\boldsymbol{\varepsilon}_{\mathrm{p}}=\begin{pmatrix}\varepsilon_x & 0 & i\varepsilon_{xz}\\ 0 & \varepsilon_y & 0\\ -i\varepsilon_{xz} & 0 & \varepsilon_x\end{pmatrix}, \tag{1}$$

where[33]

$$\varepsilon_x=1-\frac{\omega_p^2(\omega+i\nu_c)}{\omega[(\omega+i\nu_c)^2-\omega_c^2]}, \tag{2}$$

$$\varepsilon_y=1-\frac{\omega_p^2}{\omega(\omega+i\nu_c)}, \tag{3}$$

$$\varepsilon_{xz}=\frac{i\omega_p^2\omega_c}{\omega[(\omega+i\nu_c)^2-\omega_c^2]}. \tag{4}$$

The plasma frequency[33] ω_p satisfies $\omega_p=(ne^2/\varepsilon_0 m_e)^{1/2}$. The ε_0, e, and m_e represent the dielectric constant in the vacuum, electron charge, and the mass of an electron, separately. n is regarded as the carrier density for plasma, and it can be controlled in the order of magnitudes from 10^{13} to 10^{15} [43]. In this work, the carrier density n for plasma is set to 4×10^{15} m^{-3} [43]. The collision frequency of the carrier is ν_c, and its value is $0.05\omega_p$[33,44] The electron gyration frequency ω_c can be given as[33]:

$$\omega_c=\frac{eB_0}{m_e}. \tag{5}$$

For TE and TM modes, the effective dielectric constants of plasma are respectively considered as $\varepsilon_{\mathrm{TE}}$ and $\varepsilon_{\mathrm{TM}}$. They are stated as[33,35]:

$$\varepsilon_{\mathrm{TE}}=\varepsilon_y, \tag{6}$$

$$\varepsilon_{\mathrm{TM}}=\frac{\varepsilon_x^2-\varepsilon_{xz}^2}{\varepsilon_x}. \tag{7}$$

The RI of plasma can be regarded as $n_{\mathrm{TE}}=(\varepsilon_{\mathrm{TE}})^{1/2}$ and $n_{\mathrm{TM}}=(\varepsilon_{\mathrm{TM}})^{1/2}$ [33,35].

ACCEPTED MANUSCRIPT
Physics of Fluids
AIP Publishing
This is the author's peer reviewed, accepted manuscript. However, the online version of record will be different from this version once it has been copyedited and typeset.
PLEASE CITE THIS ARTICLE AS DOI: 10.1063/5.0249587

C. The RIs of E7 liquid crystal in TE and TM modes

If the temperature T_0 is constant, the values of n_e and n_o are also almost unchanged when the wavelength of EWs is from 10 μm to 1×10^4 μm[45]. In the case of T_0=300 K, the n_e and n_o of E7[45,46], a liquid crystal mixture used in this work, respectively are 1.68 and 1.50[46]. Because liquid crystal is regarded as a cylinder, the effective RI of liquid crystal depends on its long molecular axis (cylinder axis) pointing. The angle between the cylinder axis and z-axis is considered as θ. When no electric field is applied, Fig. 1(c) shows, that direction is along the y-axis (that is θ=90°). So, the effective RI of TM mode (n_{LCTM}) is equal to n_o, and the effective RI of TE mode (n_{LCTM}) is changed to n_e[46]. If applying an electric field and making the value of θ reach 0°, as displayed in Fig. 1(c), the cylinder axis is parallel to the z-axis. So, the effective RI of TM mode (n_{LCTM}) is unchanged and it is equal to n_o. The effective RI of TE mode (n_{LCTM}) is changed to n_o[46]. TABLE III lists in detail the effective RIs of different states. The value of θ can be varied by the strength of applying the electric field. This paper assumes that the electric field strength in the case of θ=0° is E_m V/m.

TABLE III The effective RIs of different states (T_0=300 K)

	TE mode	**TM mode**
$\boldsymbol{\theta}$**=0°**	n_{LCTE}=1.50 (n_o)	n_{LCTM}=1.50 (n_o)
$\boldsymbol{\theta}$**=90°**	n_{LCTE}=1.68 (n_e)	n_{LCTM}=1.50 (n_o)

D. The formula of transfer matrices and CPA

Since this work only studies the case of perpendicular incidence, the transfer matrix of the anisotropic dielectric (plasma and liquid crystal) becomes the same as that of the isotropic dielectric (TPX and Si). Moreover, the transfer matrices for TE and TM modes are also the same. Their transfer matrix can be given as[38]:

$$\mathbf{M}_j=\begin{pmatrix}\cos(k_j d_j) & -\dfrac{i}{\eta_j}\sin(k_j d_j)\\ -i\eta_j\sin(k_j d_j) & \cos(k_j d_j)\end{pmatrix}, \tag{8}$$

where $k_j=\omega/cn_i$ is the wave vector, and j is signified by different dielectric layer materials A, B, C, and D. i can be indicated by A, B, TE, TM, LCTE, and LCTM, which are regarded as different RIs. The $\eta_j=(\varepsilon_0/\mu_0)^{1/2}n_j\cos\theta_j$ is electromagnetic admittance and $\cos\theta_j$ in this paper are equal to 1. The entire matrix (**M**) of the proposed ELM can be written as[35]:

$$\mathbf{M}=\prod\mathbf{M}_j, \tag{9}$$

which can also be represented as a 2×2 matrix[35]:

$$\mathbf{M}=\begin{pmatrix}\mathbf{M}_{11} & \mathbf{M}_{12}\\ \mathbf{M}_{21} & \mathbf{M}_{22}\end{pmatrix}. \tag{10}$$

The transmission coefficient t and the reflection coefficient r can be calculated by the following formula[35]:

$$r=\frac{\eta_0(\mathbf{M}_{11}+\eta_0\mathbf{M}_{12})-(\mathbf{M}_{21}+\eta_0\mathbf{M}_{22})}{\eta_0(\mathbf{M}_{11}+\eta_0\mathbf{M}_{12})+(\mathbf{M}_{21}+\eta_0\mathbf{M}_{22})}, \tag{11}$$

$$t=\frac{2\eta_0}{\eta_0(\mathbf{M}_{11}+\eta_0\mathbf{M}_{12})+(\mathbf{M}_{21}+\eta_0\mathbf{M}_{22})}, \tag{12}$$

ACCEPTED MANUSCRIPT
Physics of Fluids
AIP Publishing
This is the author's peer reviewed, accepted manuscript. However, the online version of record will be different from this version once it has been copyedited and typeset.
PLEASE CITE THIS ARTICLE AS DOI: 10.1063/5.0249587

where $\eta_0=(\varepsilon_0/\mu_0)^{1/2}n_0$. Because the ELM is exposed to the air, the value of n_0 is equal to 1, which is the RI of air. The intrinsic reflectivity (R), the intrinsic transmissivity (T), and the intrinsic absorptivity A of the ELM can be given as[35]:

$$R=|r|^2, \tag{13}$$

$$T=|t|^2, \tag{14}$$

$$A=1-R-T. \tag{15}$$

The r and t of the positive scale are symbolized as "r_+" and "t_+". The r and t of the negative scale are regarded as "r_-" and "t_-". Because the given ELM has a symmetrical structure, there are $r=r_+=r_-$ and $t=t_+=t_-$. The observed EWs of positive and negative scales (O_+ and O_-) are both made up of the transmitted EWs from the opposite side and the reflected EWs from this side. Using the scattering matrix $\mathbf{S}$ can explain this relationship[35]:

$$\begin{pmatrix} O_+ \\ O_- \end{pmatrix}=\mathbf{S}\begin{pmatrix} I_+ \\ I_- \end{pmatrix}=\begin{pmatrix} r & t \\ t & r \end{pmatrix}\begin{pmatrix} I_+ \\ I_- \end{pmatrix}, \tag{16}$$

where I_+ and I_- are defined as the intensities of EWs from positive and negative scales.

Eq.(16) can also be expressed as[36]:

$$O_+=r|I_+|e^{i\varphi_+}+t|I_-|e^{i\varphi_-}, \tag{17}$$

$$O_-=t|I_+|e^{i\varphi_+}+r|I_-|e^{i\varphi_-}, \tag{18}$$

where φ_+ and φ_- are the phases of the EWs from positive and negative scales. The coherent absorptivity A_c can be given as[36]:

$$A_c=1-\frac{|O_+|^2+|O_-|^2}{|I_+|^2+|I_-|^2}. \tag{19}$$

So, according to Eqs.(17)-(19), the formula about A_c can be derived as:

$$A_c=1-(|t|-|r|)^2-2|t||r|\left(1+\frac{2|I_+||I_-|\cos\Delta\varphi_1\cos\Delta\varphi_2}{|I_+|^2+|I_-|^2}\right), \tag{20}$$

where $\Delta\varphi_1$=Arg(t)-Arg(r), and $\Delta\varphi_2=\varphi_+-\varphi_-$. Arg($t$) and Arg($r$) are regarded as the arguments of t and r.

III. ANALYSIS AND DISCUSSION

A. The generation of sharp TP and AP

In this work, forming sharp TP and AP is the basis for implementing logical operations. Calculating Q is an important method for evaluating the sharpness of peaks, and its formula is written as[47]:

$$Q=\frac{f_T}{FWHM}, \tag{21}$$

where f_T is the frequency point of TP or AP, and $FWHM$ is regarded as the full-width half-maximum of the homologous peak[47]. A higher Q implies that the ELM has a better selectivity.

In the case of the EWs 1 illuminating the ELM, a sharp TP forms at 7.915 GHz when one of the two electric fields (E_1 and E_2) exists, as shown in Fig. 2(a). The T at the frequency can reach 0.9. The Q of the TP is up to 2.3×10^4. There is also a sharp AP at the same frequency point in the case of $\Delta\varphi_2=180°$ and $B_0=0.23$ T when CPA occurs between EWs 1 and EWs 3. Because the phase and intensity satisfy the conditions of CPA, as displayed in Fig. 2(c), the A_c can reach 1.0 at 7.915 GHz even though the A of the ELM is only 0.5. Furthermore, the Q of the AP is up to 1.2×10^4, which is relatively high. The

ACCEPTED MANUSCRIPT
Physics of Fluids
AIP Publishing
This is the author's peer reviewed, accepted manuscript. However, the online version of record will be different from this version once it has been copyedited and typeset.
PLEASE CITE THIS ARTICLE AS DOI: 10.1063/5.0249587

circularly polarized EWs 1 becomes linearly polarized EWs 2 under the combined effect of linearly polarized EWs 3 and the given ELM. This is the fascinating aspect of combining CPA and virtual polarizer. Fig. 2(d) shows that the value of $\Delta\varphi_2$ plays an important role in forming higher A_c. For the ELM at 7.915 GHz in the case of $\Delta\varphi_2$=180°, the A_c is the highest, up to 1.0. Whether $\Delta\varphi_2$ grows positively or negatively in the range of 0°~360°, A_c decreases accordingly.

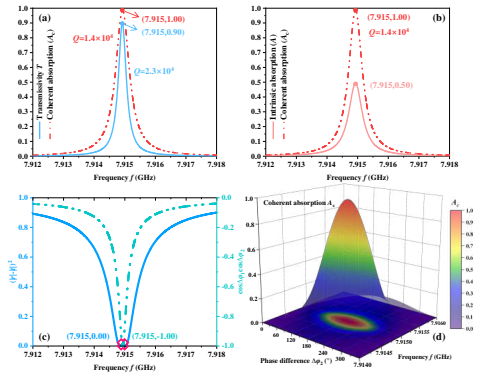

Fig. 2. Theoretical data diagrams of TP and AP. (a) The curves of T and A_c when one of E_1 and E_2exist, $\Delta\varphi_2$=180°, and B_0=0.23 T. (b) The curves of A and A_c in the case of $\Delta\varphi_2$=180° and B_0=0.23 T. (c) The curves of $\cos\Delta\varphi_1\cos\Delta\varphi_2$ and $(|r|-|t|)^2$ in the case of $\Delta\varphi_2$=180°. (d) The effects of the $\Delta\varphi_2$ and EWs frequency on the A_c.

B. Parameters optimization

Since the ELM performs logical operations with the assistance of TP and AP, the closer the values are to 1, the better the performance. To achieve better performance, various results can be obtained by adjusting parameters and comparing them, as demonstrated in Fig. 3. The influence of N_0 on TP and AP is significant (Supplement material section 2 provides detailed curves), as shown in Fig. 3(a). Although in the range of 10 to 14, TP decreases as N_0 increases. In the case of N_0=12, TP remains at a relatively high level, T=0.9. When N_0 is set to 12, the A_c reaches its maximum value of 1. However, when N_0 is increased or decreased to 14 or 10, respectively, A_c drops to about 0.7 and 0.6. As both A_c and T exhibit satisfactory values when N_0=12, the period number of stacking is defined as 12 in this paper. Fig. 3(b) illustrates that the strength of B_0 also affects the outcome of AP when N_0 is set to 12. In the case of B_0=0.23 T, A_c is up to 1, and the frequency point of AP is 7.915 GHz which is the same as TP. So, the function of a virtual polarizer can be realized by setting B_0 0.23 T.

C. The analysis of the physical mechanism of sharp AP

To clearly understand the cause of peak formation, the electric field intensity distribution maps are provided under different conditions in Fig. 4. When E_2 exists but E_1 does not, as displayed in Fig. 4(a), the plasma layer is considered as the defect layer in the ELM, leading to energy localization within this layer[48,49]. Due to this energy localization, the ELM forms a sharp TP at 7.915 GHz[50]. When only EWs 1 incidents from the positive side, there is no significant energy localization, as shown in the first map of Fig. 4(b). However, when EWs 1 and TM mode EWs 3 respectively incident from the positive and negative sides in the case of $\Delta\varphi_2$=180°, as observed in the second map of Fig. 4(b), there is significant energy localization in the middle of the ELM. Because the phase and amplitude conditions of CPA are perfectly satisfied. The energy of EWs 1 and

ACCEPTED MANUSCRIPT
Physics of Fluids
AIP Publishing
This is the author's peer reviewed, accepted manuscript. However, the online version of record will be different from this version once it has been copyedited and typeset.
PLEASE CITE THIS ARTICLE AS DOI: 10.1063/5.0249587

3 is locked in ELM and enables a more thorough energy exchange with ELM. The value of A_c can be up to 1 when $\Delta\varphi_2$ is defined as 180° in the case of B_0=0.23 T. Conversely, despite being incident through double ports, the third map of Fig. 4(b) shows that mismatched phases will disrupt the energy localization in the defect layer. If $\Delta\varphi_2$ is defined as 0°, the value of A_c will drop to 0, as demonstrated in Fig. 2(d).

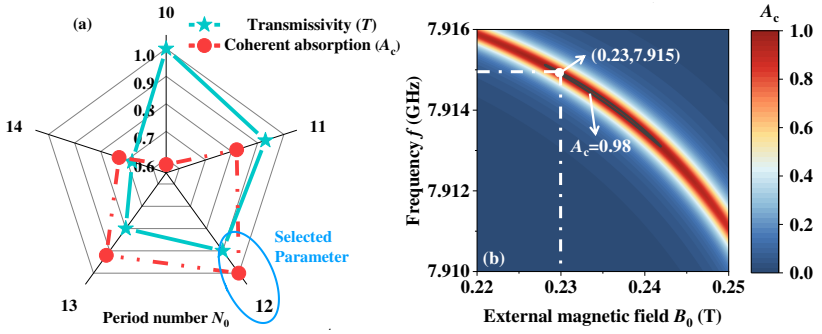

Fig. 3. The effects of different N_0 and B_0 on the results of TP and AP. (a) The peak values of A_c and T in the case of N_0=10, 11, 12, 13, and 14 when the value of B_0 is set to 0.23 T. (b) The top view of AP varies with the value of B_0 when the value of N_0 is defined as 12.

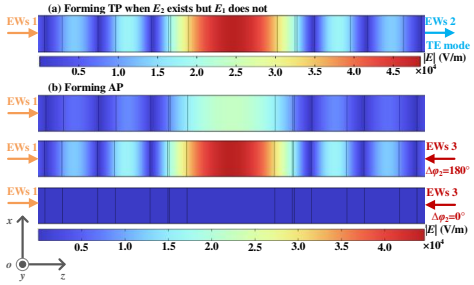

Fig. 4. The electric field intensity distribution maps about peaks forming. (a) TE mode EWs 2 transmits and form TP when E_2 exists but E_1 does not. (b) TM mode EWs 3 incidents in the case of B_0=0.23 T under three different conditions and form AP when $\Delta\varphi_2$ is defined as 180°.

D. The logical operation as a half-adder or a half-subtractor

The EWs 2 and EWs 3 display their distinctive propagation characteristics by controlling the electric fields E_1 and E_2 and magnetic field B_0 applying to liquid crystal and plasma. In addition, because there is CPA between EWs 1 and EWs 3, the phase $\Delta\varphi_2$ is also an important parameter for controlling the absorption characteristics of EWs 3. The spectrum charts satisfy the "AND" logic and the "XOR" logic, respectively, when "E_1, E_2, B_0, $\Delta\varphi_2$" are considered as the inputs and the responses of EWs 2 and 3 are the outputs.

In both half addition and half subtraction operations, the "X=1 or X=0" and "Y=1 or Y=0" of the Sum operation and the Difference operation are defined as "E_1=E_m V/m or E_1=0 V/m" and "E_2=E_m V/m and E_2=0 V/m". The two bits S and D are output with the help of TP. If T is larger than 0.9, the output level is regarded as "1". In contrast, the output level is defined as "0" when T is lower than 0.1. The difference between a half-adder and a half-subtractor is that one outputs C and the other outputs B. The working mode of the proposed ELM (a half-adder or a half-subtractor) can controlled by changing phase difference $\Delta\varphi_2$. When the "X=1 or X=0" is defined as

ACCEPTED MANUSCRIPT
Physics of Fluids
AIP Publishing
This is the author's peer reviewed, accepted manuscript. However, the online version of record will be different from this version once it has been copyedited and typeset.
PLEASE CITE THIS ARTICLE AS DOI: 10.1063/5.0249587

"$\Delta\varphi_2$=180° or $\Delta\varphi_2$=0°", the ELM is working as a half-adder. If the "X=1 or X=0" is regarded as "$\Delta\varphi_2$=0° or $\Delta\varphi_2$=180°", the ELM is a half-subtractor. The "Y=1 or Y=0" of half addition and half subtraction operations are both considered as "B_0=0.23 T or B_0=0 T".

By controlling the values of E_1, E_2, B_0, and $\Delta\varphi_2$, obtain Fig. 5, composed of different curves representing various logical outputs. As depicted in Fig. 5(a), a TP (T>0.9) occurs when either "X=1, Y=0" or "X=0, Y=1", resulting in output S or D being "1". Conversely, when the logical output S or D should be "0", no TP appears between 7.912 GHz to 7.918 GHz, with T being less than 0.1. The curves in Fig. 5(a) prove that the logical operation, functioning in TE mode, can be expressed by Eq.(22). In Fig. 5(b) and (c), it is evident that a sharp AP forms when there is a carry in X add Y or a borrow in X minus Y, denoted as "C=1" or "B=1". If no carrying or borrowing is required, no peak is observed in the range of 7.912 GHz to 7.918 GHz. In the scenario of "C=0" or "B=0", the values of A_c are below 0.1. The A_c exceeds 0.9 when the logic level of C or B transitions to "1". Fig. 5(b) and 5(c) show that Eq.(23) can describe the logical operation, working in TE mode. To more clearly analyze the logical operation, the truth table corresponding to E_1, E_2, B_0, and $\Delta\varphi_2$ is displayed in TABLE IV. The two operations can also be a flow chart, shown in Fig. 6.

$$S = D = \overline{X}Y + X\overline{Y}, \tag{22}$$

$$C = XY, B = \overline{X}Y. \tag{23}$$

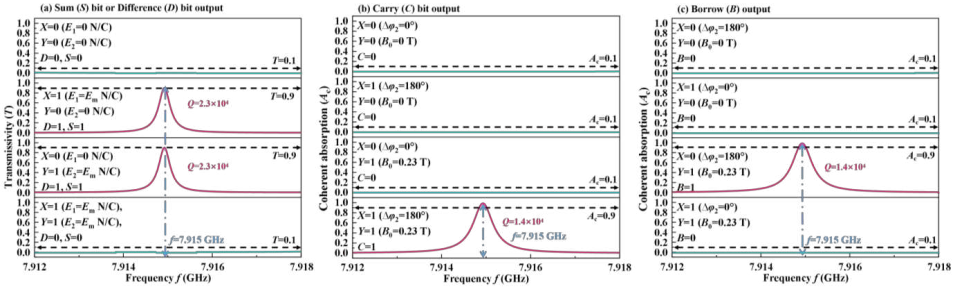

Fig. 5. The schematic curves for logical operations. (a) The operation of Sum or Difference output in TE mode in the case of X add Y or X minus Y. (b) The operation of Carry output in TM mode in the case of X add Y. (c) The operation of Borrow output in TM mode in the case of X minus Y.

TABLE IV The truth table corresponding to the variable parameters

TE mode			**TM mode**					
			a half-adder			**a half-subtractor**		
X	***Y***	***S* or *D***	***X***	***Y***	***C***	***X***	***Y***	***B***
0 (E_1=0 N/C)	0 (E_2=0 N/C)	0 (T<0.1)	0 ($\Delta\varphi_2$=0°)	0 (B_0=0 T)	0 (A_c<0.1)	0 ($\Delta\varphi_2$=180°)	0 (B_0=0 T)	0 (A_c<0.1)
1 (E_1=E_m N/C)	0 (E_2=0 N/C)	1 (T>0.9)	1 ($\Delta\varphi_2$=180°)	0 (B_0=0 T)	0 (A_c<0.1)	1 ($\Delta\varphi_2$=0°)	0 (B_0=0 T)	0 (A_c<0.1)
0 (E_1=0 N/C)	1 (E_2=E_m N/C)	1 (T>0.9)	0 ($\Delta\varphi_2$=0°)	1 (B_0=0.23 T)	0 (A_c<0.1)	0 ($\Delta\varphi_2$=180°)	1 (B_0=0.23 T)	1 (A_c>0.0)
1 (E_1=E_m N/C)	1 (E_2=E_m N/C)	0 (T<0.1)	1 ($\Delta\varphi_2$=180°)	1 (B_0=0.23 T)	1 (A_c>0.9)	1 ($\Delta\varphi_2$=0°)	1 (B_0=0.23 T)	0 (A_c>0.1)

ACCEPTED MANUSCRIPT
Physics of Fluids
AIP Publishing
This is the author's peer reviewed, accepted manuscript. However, the online version of record will be different from this version once it has been copyedited and typeset.
PLEASE CITE THIS ARTICLE AS DOI: 10.1063/5.0249587

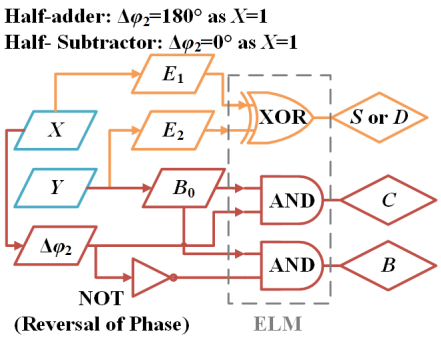

Fig. 6. The flow chart of the ELM working as a half-adder or a half-subtractor.

Moreover, the realization of a logic function based on a virtual polarizer is an innovation point of this work. AxisRatio (*AR*) is an important performance index of circular polarization. If *AR* of EWs is not greater than 3 dB, the EWs is defined as circular polarization[51]. The formula of *AR* is written as[51]:

$$AR(\mathrm{dB}) = \left| 20\log_{10}\left\{ \tan\left[\frac{2O_{\mathrm{TM}}O_{\mathrm{TE}}}{O_{\mathrm{TM}}^{\ 2}+O_{\mathrm{TE}}^{\ 2}} \sin(\Delta\varphi) \right] \right\} \right|, \tag{24}$$

where O_{TE} and O_{TM} respectively are observed EWs of TE mode and TM mode, and $\Delta\varphi$ is regarded as the phase difference between them. Fig.7 shows the *AR* of negative observed EWs in different logical states (For clarity, *AR* is represented by a negative number). When the output is "*S*=0, *C*=0" or "*D*=0, *B*=0", the *AR* is less than -40 dB and the EWs are close to ideal linear polarization. There is a frequency point *AR* is close to 0 dB when the output is "*S*=1, *C*=0" or "*D*=1, *B*=0". *AR* is larger than -40 dB but much less than 0 dB in the case of "*S*=0, *C*=1" or "*D*=0, *B*=1". If the output is "*S*=1, *C*=1" or "*D*=1, *B*=1", there are two frequency points *AR* is close to 0 dB. The ELM operation results can be clearly obtained through the polarization of EWs, which greatly speeds up the ELM operation efficiency.

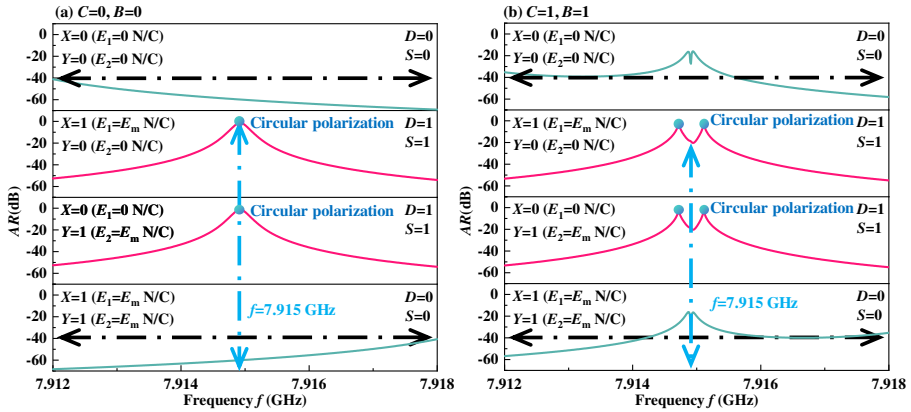

Fig. 7. The schematic curves of *AR* in different logical operations. (a) the output of "AND" logical operation is "0". (b) the output of "AND" logical operation is "1".

ACCEPTED MANUSCRIPT
Physics of Fluids
AIP Publishing
This is the author's peer reviewed, accepted manuscript. However, the online version of record will be different from this version once it has been copyedited and typeset.
PLEASE CITE THIS ARTICLE AS DOI: 10.1063/5.0249587

E. Numerical verification

Experiment is an indispensable link to verify the correctness of the work. However, due to the lack of experimental conditions, it is unrealistic to prepare samples for real experiments. To make this work more complete, simulation experiments were carried out with the simulation software, HFSS. The Floquet ports at the top and bottom of the unit, respectively, are where the vertically incident coherent EWs are released. In , the primary-secondary mode is used for the boundary conditions. As can be seen in Fig. 8, the HFSS results and the theoretical results are both frequency-shifted for different logical states. Fig. 9 displays that a sharp AP only occurs in the case of "1 AND 1" whether it is a theoretical result or a HFSS result.

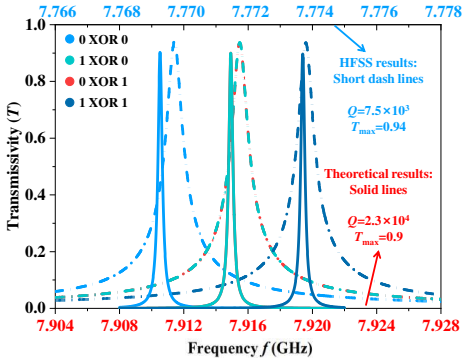

Fig. 8. TP in different logical states (the red *f*-axis corresponds to theoretical results and the bule *f*-axis corresponds to HFSS results).

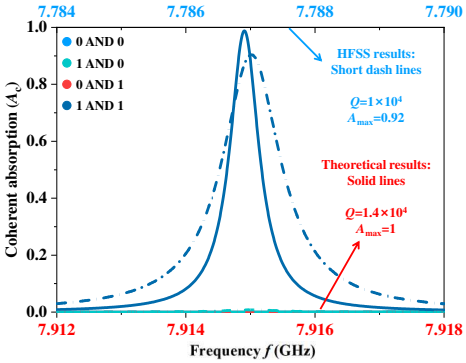

Fig. 9. AP in different logical states (the red *f*-axis corresponds to theoretical results and the bule *f*-axis corresponds to HFSS results).

While the formula in this study is based on the analytical solution approach, HFSS is based on the finite element method. There are discrepancies in the simulation results generated by different approaches due to the truncation error in the data value calculation, for instance, the characteristic frequencies do not coincide completely. The accuracy of HFSS depends on mesh density—coarse grids may cause frequency shifts and Q errors, while dense grids improve accuracy at the cost of longer computation times and more computer memory. Moreover, analytical methods like the transfer matrix method are efficient and allow fine frequency step control (e.g., 1^{-6} GHz), whereas the numerical methods may introduce deviations due to coarse frequency steps. The maximum inaccuracy of the two simulation approaches after computation is 0.143 GHz. The error of 0.143 GHz is only 1.8% when compared to the frequency band in which this ELM operates. Compared with the theoretical value, although the performance parameters of ELM have decreased in the simulation experiment, it is still satisfactory.

ACCEPTED MANUSCRIPT
Physics of Fluids
AIP Publishing
This is the author's peer reviewed, accepted manuscript. However, the online version of record will be different from this version once it has been copyedited and typeset.
PLEASE CITE THIS ARTICLE AS DOI: 10.1063/5.0249587

F. Performance analysis

TABLE V The published electromagnetic logic devices compared with this work in performance

Refs.		*SNR* (dB)	*Q*	Logical function	Arithmetical operation	Virtual Polarizer	CPA	Phase control
[52]		8.2	77	NOR & AND	×	×	×	×
[53]		4.5	-	XOR & AND	Half-adder	×	×	×
[54]		6.0	-	OR &AND	×	×	×	×
[55]		6.5	9	NOT, NOR, OR, & AND	×	×	×	×
[56]		-	-	OR, NOR, XOR, & AND	×	×	×	×
[57]		2.07	-	AND, OR, XOR, NAND, NOR, XNOR, & NOT	×	×	×	×
[58]		5.77	-	NOT, NOR, & AND	×	×	×	×
THIS WORK	TE mode	9.7	7.5×10^3	XOR	Half-adder & Half-subtractor	√	×	√
	TM mode	30.0	1×10^4	AND or BORROW			√	

The dependability of ELMs is assessed through the use of the *SNR* [34]. The formula of *SNR* is regarded as [34]:

$$SNR(\mathrm{dB}) = 10\log_{10}\left(\frac{A_1}{A_0}\right), \tag{26}$$

where the values of A_c at an output value of "1" or "0" are represented individually by A_1 and A_0. "*SNR*=3 dB" is considered to be the cutoff point between low and high *SNR*s.

The higher the *SNR*, the better the calculation accuracy of the logic device [34]. The *SNR* of the proposed electromagnetic half-subtractor is listed in TABLE V. Furthermore, TABLE V incorporates several previous studies on electromagnetic logic devices, systematically illustrating the advantages of this work. In comparison with these published studies, our work advances beyond logical operations into arithmetic operations. The achieved improvements in *SNR* and *Q* endow the proposed ELM with outstanding performance, meeting the requirements of a half-adder or a half-subtractor. Leveraging the technique of CPA, the ELM gains the capability of changing operation type by controlling phase. Additionally, this work combines the function of a virtual polarizer with arithmetic operations in an ELM, which provides a new idea for the study of ELM and virtual polarizer. It is of great significance for the development of the antennas and propagation community.

IV. CONCLUSION

In summary, the proposed ELM functions as an electromagnetic half-adder or half-subtractor, capable of outputting "*S* and *C*" or "*D* and *B*" simultaneously. The use of two anisotropic materials (liquid crystal and plasma) enables EWs to exhibit distinct propagation characteristics in different polarization directions. In TE mode, input logic levels are controlled by adjusting applied electric fields (E_1 and E_2). When the output level is "1", a sharp TP is observed, with *T* exceeding 0.9. For TM mode, the phase and applied magnetic field serve as input parameters. When these coherent EWs satisfy the conditions for CPA, denoted as "*C*=1" or "*B*=1," a sharp AP is generated by the ELM, with A_c reaching a value of 1. With enhanced *SNR* and high *Q* (28 dB and at least 1.4×10^4), this ELM achieves high-accuracy calculations. Because the ELM based on virtual polarizer realizes parallel processing of AND logic and XOR logic, faster information encryption operation may be realized. Compared with traditional ELM, this work improves the complexity and performance of electromagnetic calculation through parallel logic operation.

ACCEPTED MANUSCRIPT
Physics of Fluids
AIP Publishing
This is the author's peer reviewed, accepted manuscript. However, the online version of record will be different from this version once it has been copyedited and typeset.
PLEASE CITE THIS ARTICLE AS DOI: 10.1063/5.0249587

SUPPLEMENTARY MATERIAL

See the supplementary material for the introduction of liquid crystal, preparation methods, and detailed curves of TP and AP in different N_0.

ACKNOWLEDGMENTS

This work was supported by the National College Students Innovation and Entrepreneurship Training Program (Grant No.202410293018Z).

CONFLICT OF INTEREST

The authors declare no conflicts of interest.

DATA AVAILABILITY STATEMENT

The data that support the findings of this study are available from the corresponding author upon reasonable request.

REFERENCES

[1] H. Jiang, Y. Chen, G. Li, C. Zhu, and X. Chen, *Opt. Express* **23**, 9784–9789 (2015).
[2] M. A. Butt, S. N. Khonina, and N. L. Kazanskiy, *Opt. Laser Technol.* **142**, 107265 (2021).
[3] Y. Fu, X. Hu, C. Lu, S. Yue, H. Yang, and Q. Gong, *Nano Lett.* **12**, 5784–5790 (2012).
[4] J. Xu, C. Zhang, Y. Wang, M. Wang, Y. Xu, T. Wei, and L. Zhou, *Nat Commun*, **15**, 1726 (2024).
[5] R. W. Hamming, *Bell Syst. Tech. J.* **29**, 147–160 (1950).
[6] J. Wang, J. Sun, and Q. Sun, *Opt. Express* **15**, 1690–1699 (2007).
[7] K. Mukherjee, *Optik* **122**, 1188–1194 (2011).
[8] Wang, J., Sun, J., and Sun, Q., *Opt. Express* **15**, 1690-1699 (2007).
[9] F. Parandin, S. Olyaee, F. Heidari, M. Soroosh, A. Farmani, H. Saghaei, and A. Ehyaee, *J. Opt. Commun*, (2024).
[10] Y. Huang, T. Xiao, S. Chen, Z. Xie, J. Zheng, J. Zhu, and L. Li, *OEA* **6**, 220073–220073 (2023).
[11] Q. Q. Li and H. F. Zhang, *IEEE Trans. Antennas Propag.* **71**, 3033–3041 (2023).
[12] Y. P. Li, Z. Qiao, K. Xia, L. Zhang, and H. F. Zhang, *IEEE Trans. Antennas Propag.* **71**, 8097–8110 (2023).
[13] C. Huang, W. Pan, X. Ma, and X. Luo, *IEEE Trans. Antennas Propag.* **64**, 1173–1178 (2016).
[14] A. K. Iyer, A. Alù, and A. Epstein, *IEEE Trans. Antennas Propag.* **68**, 1223–1231 (2020).
[15] M. C. Tang, Z. Chen, H. Wang, M. Li, B. Luo, J. Wang, and R.-W. Ziolkowski, *IEEE Trans. Antennas Propag.* **65** 3986–3998 (2017).
[16] J. Y. Sui, S. Liao, B. Li, and H. F. Zhang, *Opt. Lett.* **47**, 6065–6068 (2022).
[17] Q. Yang, H. Xiong, J. H. Deng, B. X. Wang, W. X. Peng, and H. Q. Zhang, *Appl. Phys. Let.* **122**, 253901 (2023).
[18] C. Gigli, G. Marino, A. Artioli, D. Rocco, C. De Angelis, J. Claudon, and G. Leo, *Optica* **8**, 269–276 (2021).
[19] F. Capolino, M. Khajavikhan, and A. Alù, *Appl. Phys. Lett.* **120**, 060401 (2022).
[20] Z. Zheng, Y. Huang, F. Wu, H. Zhang, and Z. Fang, *Sci. China Inf. Sci.* **66**, 160403 (2023).
[21] M. Pishvar and R. L. Harne, *Adv. Sci.* **7**, 2001384 (2020).
[22] P. Thureja, R. Sokhoyan, C.-U. Hail, J. Sisler, M. Foley, M.-Y. Grajower, and H.-A. Atwater, *Nanophotonics* **11**, 3745–3768 (2022).

ACCEPTED MANUSCRIPT
Physics of Fluids
AIP Publishing
This is the author's peer reviewed, accepted manuscript. However, the online version of record will be different from this version once it has been copyedited and typeset.
PLEASE CITE THIS ARTICLE AS DOI: 10.1063/5.0249587

[23] N. Mohammadi Estakhri, B. Edwards, and N. Engheta, *Science* **363**, 1333–1338 (2019).
[24] J. Chen, S. Hu, S. Zhu, and T. Li, *Interdisciplinary Materials* **2**, 5–29 (2023).
[25] Y. D. Chong, L. Ge, H. Cao, and A. D. Stone, *Phys. Rev. Lett.* **105**, 053901 (2010).
[26] D. G. Baranov, A. Krasnok, T. Shegai, A. Alù, and Y. Chong, *Nat. Rev. Mater.* **2**, 1–14 (2017).
[27] D. Yan, R. Mei, M. Li, Z. Ma, Z. H. Hang, and J. Luo, *Nanophotonics*, **12**, 4195–4204 (2023).
[28] Hasegawa, M., Oi, J., Yamashita, K., Seto, K., Kobayashi, T., and Tokunaga, E., *Langmuir* **39**, 11357-11362 (2023).
[29] M. Markowitz, E. Vela, A. K. Jahromi, M. C. Tamargo, I. L. Kuskovsky, and M.-A. Miri, *Opt. Express* **31**, 28285–28294 (2023).
[30] P. Qiao, W. Yang, and C. J. Chang-Hasnain, *Adv. Opt. Photon.* **10**, 180–245 (2018).
[31] Y. R. Wu, R. Y. Dong, and H. F. Zhang, *IEEE Trans. Antennas Propag.* **72**, 1–1 (2024).
[32] H. Yang, K. Ou, H. Wan, Y. Hu, Z. Wei, H. Jia, and H. Duan, *Materials Today* **67**, 424–445 (2023).
[33] L. Qi, Z. Yang, F. Lan, X. Gao, and Z. Shi, *Phys. Plasmas* **17**, 042501 (2010).
[34] D. H. Johnson, *Scholarpedia* **1**, 2088 (2006).
[35] L. Qi, Z. Yang, F. Lan, X. Gao, and Z. Shi, *Phys. Plasmas* **17**, 042501 (2010).
[36] W. Zhu, F. Xiao, M. Kang, and M. Premaratne, *Appl. Phys. Lett.* **108**, 121901 (2016).
[37] Z. Li and K. Aik Khor, *Encyclopedia of Biomedical Engineering*, 203–212 (2019).
[38] V. A. Tolmachev, E. V. Astrova, J. A. Pilyugina, T. S. Perova, R. A. Moore, and J. K. Vij, *Opt. Mater.* **27**, 831–835 (2005).
[39] M. Naftaly, R. E. Miles, and P. J. Greenslade, *2007 Joint 32nd International Conference on Infrared and Millimeter Waves and the 15th International Conference on Terahertz Electronics*, 819–820 (2007).
[40] X. Ma, J. Wu, L. Jiang, M. Wang, G. Deng, S. Qu, and K. Chen, *Lab Chip*, **21**, 3298–3306 (2021).
[41] C. Nayak, C. G. Bezerra, and C. H. Costa, *Opt. Mater.* **104**, 109838 (2020).
[42] L. Xuan, X. Kong, J. Wu, Y. He, and Z. Xu, *Appl. Magn. Reson.* **52**, 649–660 (2021).
[43] Y. C. Jun, E. Gonzales, J. L. Reno, E. A. Shaner, A. Gabbay, and I. Brener, *Opt. Express* **20**, 1903–1911 (2012).
[44] C. D. Decker, W. B. Mori, J. M. Dawson, and T. Katsouleas, *Phys. Plasmas* **1**, 4043–4049 (1994).
[45] H. Y. Peng, Y. A. Wei, K. C. Lin, S. F. Hsu, J. C. Chen, C. P. Cheng, and C. S. Yang, *J. Opt. Soc. Am. B* **27**, 1866–1873 (2010).
[46] J. Li, S. T. Wu, S. Brugioni, R. Meucci, and S. Faetti, *J. Appl. Phys.* **97**, 073501 (2005).
[47] B. F. Wan, Q. Y. Wang, H. M. Peng, H. N. Ye, and H. F. Zhang, *IEEE Sens. J.* **21**, 21465–21472 (2021).
[48] E. Özbay, G. Tuttle, M. Sigalas, C. M. Soukoulis, and K. M. Ho, *Phys. Rev. B* **51**, 13961–13965 (1995).
[49] I. L. Lyubchanskii, N. N. Dadoenkova, A. E. Zabolotin, Y. P. Lee, and T. Rasing, *J. Opt. A: Pure Appl. Opt.* **11**, 114014 (2009).
[50] X. Zhang, G. Yu, G. Yuan, and Y. Lv, *Optic. Mater.* **114**, 110771 (2021).
[51] J.-Y. Liu, T.-J. Huang, and P.-K. Liu, *APMC*, 1142–1144 (2017).
[52] F. Parandin and M. M. Karkhanehchi, *Superlattices Microstruct.* **101**, 253–260 (2017).
[53] Y. Pugachov, M. Gulitski, O. Mizrahi, and D. Malka, *Symmetry* **15**, 1063 (2023).
[54] R. M. Younis, N. F. F. Areed, and S. S. A. Obayya, *IEEE PHOTONIC TECH L.* **26**, 1900–1903 (2014).
[55] A. Ghadi and B. Darzi, *Opt. Laser Technol.* **157**, 108651 (2023).
[56] Y. Chen, Z. Huang, J. Huang, L. Shao, F. Gao, X. Chen, and Y. Zhang, *Appl. Phys. Lett.* **122**, 033501 (2023).
[57] J. Jot Singh, D. Dhawan, and N. Gupta, *Opt. Laser Technol.* **165**, 109624 (2023).
[58] S. Soma, S. K. C. Gowre, M. V. Sonth, B. Gadgay, and B. Jyoti, *Opt. Quant. Electron.* **55**, 340 (2023).